

The Mellin Transform Technique for the Extraction of the Gluon Density

D. Graudenz¹, M. Hampel², A. Vogt^{3*}, Ch. Berger²

¹Theoretical Physics Division, CERN
CH-1211 Geneva 23, Switzerland

²I. Physikalisches Institut, RWTH Aachen
D-52056 Aachen, Germany

³Deutsches Elektronen-Synchrotron DESY
D-22603 Hamburg, Germany

Abstract

A new method is presented to determine the gluon density in the proton from jet production in deeply inelastic scattering. By using the technique of Mellin transforms not only for the solution of the scale evolution equation of the parton densities but also for the evaluation of scattering cross sections, the gluon density can be extracted in next-to-leading order QCD. The method described in this paper is, however, more general, and can be used in situations where a repeated fast numerical evaluation of scattering cross sections for varying parton distribution functions is required.

CERN-TH/95-149
June 1995

* On leave of absence from Sektion Physik, Universität München, D-80333 Munich, Germany.

Electronic mail addresses: Dirk.Graudenz@cern.ch, Hampel@desy.de, avogt@x4u2.desy.de, Berger@rwth-aachen.de.

1 Introduction

One of the main goals of experiments at the electron–proton collider HERA is the precise determination of the gluon density $f_{g/p}(\xi, \mu^2)$ in the proton for various gluon momentum fractions ξ and factorization scales μ . In addition to the indirect method of extracting $f_{g/p}$ from the scaling violation of the structure function F_2 , direct methods such as heavy quark and jet production have been studied.

In the QCD–improved parton model, the electron–proton scattering cross section σ is generically given by a convolution of process-independent parton densities $f_{q/p}$ for (anti-)quarks and $f_{g/p}$ for gluons with corresponding mass-factorized parton-level cross sections σ_q and σ_g :

$$\sigma = \int d\xi \left[f_{q/p}(\xi, \mu^2) \sigma_q(\xi, \mu^2) + f_{g/p}(\xi, \mu^2) \sigma_g(\xi, \mu^2) \right]. \quad (1)$$

Besides the indicated dependence on ξ and μ , σ_q and σ_g also depend on other variables such as the absolute electron four-momentum transfer squared Q^2 and the momenta of the outgoing partons¹.

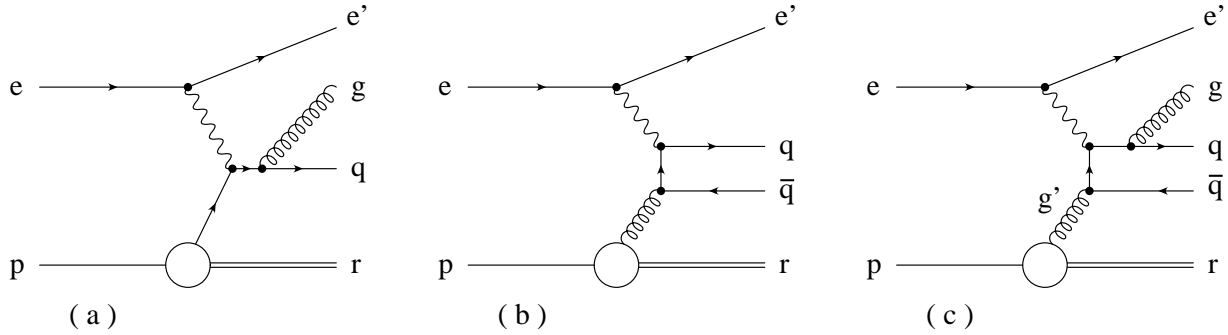


Figure 1: *Generic Feynman diagrams for the leading-order processes of QCD Compton scattering (a) and photon–gluon fusion (b), and an example for a diagram corresponding to a next-to-leading order real correction (c).*

In leading order (LO), the prescription for the extraction of $f_{g/p}$ from jet cross sections in deeply inelastic scattering reactions is very intuitive, because σ_q can be identified with the parton-model cross section σ_C for the so-called *QCD Compton scattering* process (fig. 1a), and σ_g with the parton-model cross section σ_F for the *photon–gluon fusion* reaction (fig. 1b). Explicit expressions can be found in [1]. Experimentally the outgoing partons from the hard scattering reactions are identified with jets. The QCD Compton scattering and photon–gluon fusion reactions lead to (2+1)-jet final states, where the notation accounts for the two outgoing jets from the hard scattering process and the jet in the proton fragmentation region. The calculated contribution

¹Here and in the following we do not explicitly display the dependence on the renormalization scale.

$\sigma_{C,2+1}^{\text{LO}} = \int d\xi f_{q/p}(\xi, \mu^2) \sigma_C(\xi)$ from Compton scattering can be subtracted from the measured cross section

$$\sigma_{2+1}^{\text{LO}} = \int d\xi \left[f_{q/p}(\xi, \mu^2) \sigma_C(\xi) + f_{g/p}(\xi, \mu) \sigma_F(\xi) \right], \quad (2)$$

and thus $f_{g/p}(\xi, \mu^2)$ can be determined in LO by a direct unfolding, since in this case ξ can be expressed in terms of measurable quantities as $\xi = x_B (1 + \hat{s}/Q^2)$, where x_B is the Bjorken scaling variable and \hat{s} is the invariant mass squared of the system of the two current jets. An analysis based on this principle has recently been presented by the H1 Collaboration [2].

In next-to-leading order (NLO) this simple picture is destroyed. Aside from the virtual corrections to the Born processes in figs. 1a and b, real corrections have to be added; diagrams of the type shown in fig. 1c can also lead to (2+1)-jet configurations: if the gluon g attached to the outgoing quark is soft or collinear to the quark, the diagram constitutes a correction to the photon–gluon fusion process. If, on the other hand, this gluon is hard and the outgoing antiquark \bar{q} is soft or collinear to the incoming gluon g' , then this configuration can be said to be a correction to the QCD Compton scattering reaction. In the latter case, the collinear or soft antiquark forms a jet with the proton remnant r , and the cross section has to be integrated over all momenta of the antiquark according to a specific jet definition scheme. Collinear singularities that do not cancel against corresponding singularities from the virtual corrections have to be absorbed into renormalized parton densities. Depending on the factorization scheme chosen, finite subtracted pieces remain. The factorization theorems of perturbative QCD guarantee that the cross section can be written in the form of eq. (1). However, beyond the leading order, the arbitrary momentum of collinear partons renders the variable ξ unobservable, because the mass-factorized parton-level cross sections are in general distributions, not regular functions, and the simple and straightforward method described above can therefore not be applied. A physical consequence is that the distinction between the QCD Compton and photon–gluon fusion processes becomes meaningless. Related to this is the fact that quark and gluon densities mix in the Altarelli–Parisi scale evolution.

A determination of the gluon density in NLO is very desirable. In LO the partonic cross sections σ_q and σ_g (in short denoted by σ_i) do not depend on μ , as already indicated in eq. (2), and the $f_{i/p}$ (as short-hand for $f_{q/p}$ and $f_{g/p}$) are the solutions of the LO Altarelli–Parisi evolution equation, where the leading logarithmic terms in the scale μ are summed up. In any finite order of perturbation theory, the scattering cross section σ depends explicitly on the factorization scale μ , this scale dependence being due to uncalculated higher-order terms. The scale dependence is particularly strong in the LO case, because there no compensation can take place between $f_{i/p}$ and σ_i . To a great extent this problem is, for many processes, reduced in NLO, where explicit terms $\sim \ln \mu^2$ in σ_i compensate the μ -dependence of $f_{i/p}$ such that the variation is of higher order in the strong coupling constant α_s . For reliable theoretical predictions, a NLO analysis of scale-dependent quantities is therefore mandatory.

The only way to achieve a direct NLO determination of $f_{g/p}$ is to parametrize the function

$f_{g/p}$ at a given scale μ_0 , to evolve it then to a value of μ where the cross section is measured, say $\mu = Q$, and to fit the parameters of $f_{g/p}$ with respect to suitable infrared safe observables, e.g. the (2+1)-jet cross section in various bins of x_B . A severe practical problem is that the cross section σ has to be evaluated repeatedly for every choice of parameters for $f_{g/p}$. Monte Carlo methods allow the application of arbitrary cuts on final-state particle momenta, as is necessary in order to take detector acceptance cuts properly into account, but these methods are prohibitively slow. A fast numerical method for the repeated application of this procedure is indispensable, and will be developed in this paper.

The paper is organized as follows. The new method is formally derived in Section 2. Details of the Mellin transform relevant to the application of the method are discussed in Section 3. Finally, an explicit numerical example is given in Section 4 for the case of jet cross sections in deeply inelastic electron–proton scattering, where it is shown that the method is operational in practice when realistic acceptance cuts are taken into account. The paper closes with a short summary.

2 The Mellin Transform Technique for Non-Factorizing Cross Sections

The Mellin transform technique allows for a quick numerical evaluation of integrals of the form

$$\Sigma(x_B) = \int_{x_B}^1 \frac{d\xi}{\xi} f_{i/p}(\xi) \sigma_i\left(\frac{x_B}{\xi}, x_B\right) \quad (3)$$

in the case where σ_i is independent of its second argument x_B , on the basis of the moments defined by

$$F_n \equiv \int_0^1 \frac{dx}{x} x^n F(x) \quad (4)$$

for an arbitrary function F and (complex) n . The moments of the function Σ are then given by

$$\Sigma_n = f_{i/p,n} \sigma_{i,n}. \quad (5)$$

The functional dependence of Σ can be recovered from the moments Σ_n by an inverse Mellin transform. An expression of the form of eq. (3) will be called to be of the *factorizable type* if the only dependence on x_B in the arguments of σ_i is via x_B/ξ . In the application which we have in mind, $f_{i/p}$ is a parton density, whereas σ_i is an expression for a mass-factorized parton-level scattering cross section. In general, acceptance cuts and non-factorizable jet algorithms (cf. the discussion in [3, 4]) introduce an explicit dependence of σ_i on x_B . Moreover, the expression for $\Sigma(x_B)$ is integrated over a certain range of x_B . This might suggest that the Mellin transform technique cannot be applied. However, this is not the case. In the following we outline a method that allows the use of this technique.

The cross section differential in x_B can be written in the form

$$\Sigma(x_B) = \int_{x_B}^1 \frac{d\xi}{\xi} f_{i/p}(\xi, \mu^2) \sigma_i\left(\frac{x_B}{\xi}, x_B, \mu^2\right), \quad (6)$$

where

$$\sigma_i\left(\frac{x_B}{\xi}, x_B, \mu^2\right) = \int_{V_{x_B}} dT \hat{\sigma}_i\left(\frac{x_B}{\xi}, x_B, T, \mu^2\right). \quad (7)$$

Here we have made the dependence on the factorization scale μ explicit. The set T of variables contains all other integration variables besides x_B , i.e. the other electron variables including Q^2 and the momenta of the outgoing partons (or jets); and V_{x_B} is the phase space region over which these variables are integrated. Thus, V_{x_B} includes all acceptance and jet cuts, as well as the range in Q^2 for the specified x_B . $\hat{\sigma}_i$ is the cross section differential in all variables including T , whereas σ_i is the integration kernel to be convoluted with $f_{i/p}$ to yield Σ . The explicit dependence on x_B of $\hat{\sigma}_i(x_B/\xi, x_B, T, \mu^2)$ and $\sigma_i(x_B/\xi, x_B, \mu^2)$ (not just via the ratio x_B/ξ) is a consequence of the (finite) factorization breaking terms².

It is assumed that the factorization scale μ is chosen independently from the variables T ; in particular, μ should not depend on the integration variable Q^2 , which is integrated over a certain range $[Q_0^2, Q_1^2]$. μ it may be set to some intermediate value. In any case, this is not a strong restriction, because the parton densities depend only logarithmically on the factorization scale, and moreover the scale dependence is compensated by a corresponding term in the mass-factorized parton-level scattering cross section, so that the change is of higher order in α_s . For simplicity of notation, we drop the argument μ^2 in the following.

Now let (for a fixed Q^2 -bin) a_1, \dots, a_k be the experimental boundaries of the intervals in the variable x_B for which the cross sections are measured. To proceed, we define

$$\Sigma_a \equiv \int_a^1 dx_B \Sigma(x_B). \quad (8)$$

The integral over a specified interval $[a_i, a_{i+1}]$ in x_B is then simply given by

$$\int_{a_i}^{a_{i+1}} dx_B \Sigma(x_B) = \Sigma_{a_i} - \Sigma_{a_{i+1}}. \quad (9)$$

In a fit of the function $f_{i/p}$, the integrals in eqs. (6), (7), (8) have to be evaluated repeatedly. In general, the x_B , ξ and T -integrations are performed by a time-consuming Monte Carlo integration in order to implement all cuts. In particular, the (x_B, Q^2) -plane is divided into several bins which do not change during the fitting procedure. The method requires that a certain set of moments is calculated for every bin in the (x_B, Q^2) -plane. The steps to be followed to determine the Σ_a are:

²It should be kept in mind that the infinite terms related to infrared and collinear singularities still factorize in the standard form so that universal parton densities can be defined. This property is not spoiled by acceptance cuts and non-factorizing jet definition schemes.

- Define a function

$$h_a(u) \equiv \begin{cases} \int_a^{a/u} dx_B \sigma_i \left(\frac{x_B}{a/u}, x_B \right), & \text{if } u \geq a \\ 0, & \text{if } u < a \end{cases} \quad (10)$$

and its moments in the variable u

$$h_{an} \equiv \int_0^1 \frac{du}{u} u^n h_a(u). \quad (11)$$

It is easy to prove that an explicit expression for h_{an} is

$$h_{an} = \int_a^1 dx_B \int_{x_B}^1 \frac{d\xi}{\xi} \left(\frac{a}{\xi} \right)^n \sigma_i \left(\frac{x_B}{\xi}, x_B \right). \quad (12)$$

The h_{an} are thus the Σ_a with the parton density $f_{i/p}(\xi)$ replaced by $(a/\xi)^n$. They can be determined numerically by means of a Monte Carlo integration. In general, for complex n , the quantity $(a/\xi)^n$ has to be split into its real and imaginary part.

- Define

$$\Sigma_{ab} \equiv \int_a^1 \frac{d\xi}{\xi} f_{i/p}(\xi) h_b \left(\frac{a}{\xi} \right) \quad (13)$$

and determine the moments of Σ_{ab} with respect to the variable a :

$$\tilde{\Sigma}_{nb} \equiv \int_0^1 \frac{da}{a} a^n \Sigma_{ab}. \quad (14)$$

Obviously, $\Sigma_a = \Sigma_{aa}$. The key relation of our method is

$$\tilde{\Sigma}_{nb} = f_{i/p,n} h_{bn}, \quad (15)$$

and can be proved in the following way:

$$\begin{aligned} \tilde{\Sigma}_{nb} &= \int_0^1 \frac{da}{a} a^n \int_a^1 \frac{d\xi}{\xi} f_{i/p}(\xi) h_b \left(\frac{a}{\xi} \right) \\ &= \int_0^1 \frac{d\xi}{\xi} f_{i/p}(\xi) \int_0^\xi \frac{da}{a} a^n h_b \left(\frac{a}{\xi} \right) \\ &= \int_0^1 \frac{d\xi}{\xi} \xi^n f_{i/p}(\xi) \int_0^1 \frac{du}{u} u^n h_b(u) \\ &= f_{i/p,n} h_{bn}. \end{aligned} \quad (16)$$

- For a given parametrization of $f_{i/p}$ in terms of its moments $f_{i/p,n}$ the cross section Σ_a can be determined by forming the moments $\tilde{\Sigma}_{na} = f_{i/p,n} h_{an}$ and a subsequent inverse Mellin transform in the variable n , evaluated at a .

The Mellin transform method in the case of non-factorizing cross sections introduces the inconvenience that the moments h_{an} have to be determined for every interval boundary a separately. Due to the large number of repeated cross section evaluations in the fitting procedure, however, this method is far more efficient than a direct integration of the integrals in eqs. (6), (7), (8) for every parametrized parton density.

3 From Parton Moments to Observables

Let us now consider the inverse transformation of the moments given by eq. (4), which is a special case of the general Mellin transformation for functions $F(x)$ vanishing identically at $x > 1$. If $F(x)$ is piecewise smooth for $x > 0$, the corresponding Mellin inversion reads

$$F(x) = \frac{1}{2\pi i} \int_{c-i\infty}^{c+i\infty} dn x^{-n} F_n, \quad (17)$$

where the real number c has to be chosen such that $\int_0^1 dx x^{c-1} F(x)$ is absolutely convergent [5]. Hence c has to lie to the right of the rightmost singularity n_{max} of F_n . The contour of the integration in eq. (17) is displayed in fig. 2 and denoted by \mathcal{C}_0 . Also shown is a deformed route \mathcal{C}_1 , yielding the same result as long as no singularities n_i of F_n are enclosed by $\mathcal{C}_0 - \mathcal{C}_1$. For example, for the LO and NLO evolution of structure functions, the n_i are real with $n_i < n_{max} < c$, and this requirement is fulfilled automatically.

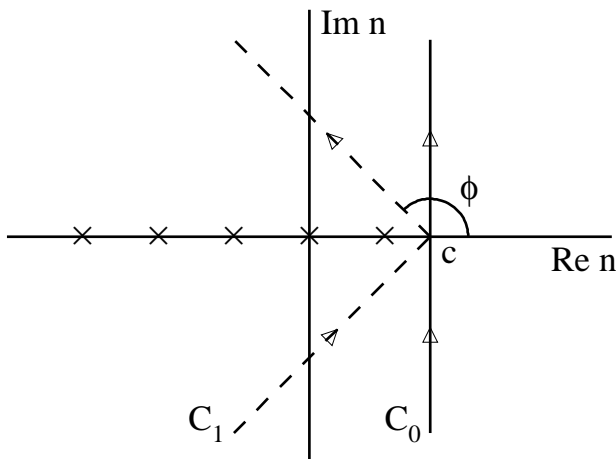


Figure 2: *Integration contours of the Mellin inversion in eq. (17), leading to the inversion formulae of eqs. (18) and (19) for the routes \mathcal{C}_0 and \mathcal{C}_1 , respectively. The crosses schematically denote the singularities of F_n .*

It is useful to rewrite eq. (17) as an integration over a real variable. We are concerned with functions obeying $F_n^* = F_{n^*}$, where ‘ $*$ ’ denotes the complex conjugation. Then it is easy to show that eq. (17) yields, for the contour characterized by the abscissa c and the angle ϕ in fig. 2:

$$F(x) = \frac{1}{\pi} \int_0^\infty dz \operatorname{Im} \left[\exp(i\phi) x^{-c-z \exp(i\phi)} F_{n=c+z \exp(i\phi)} \right]. \quad (18)$$

It is obvious from the discussion given above that the integral does not depend on c and ϕ . However, for an efficient numerical evaluation a suitable choice of these parameters is very useful. For example, it is advantageous to choose $\phi > \pi/2$ in case F_n is a known analytical function,

especially if this function does not fall off very rapidly for $|n| \rightarrow \infty$. The factor $\exp\left(z \log \frac{1}{x} \cos \phi\right)$ then introduces an exponential dampening of the integrand (which rapidly oscillates at small x) with increasing z , thereby allowing for a smaller upper limit z_{max} in the numerical implementation of eq. (18). This procedure has been employed for the inversion of moments of parton densities and structure functions for the proton and the photon, e.g. in [6, 7] and [8], respectively.

In general, however, the moments of the partonic cross section can only be calculated numerically using eq. (4), because no analytic continuation to small $\text{Re } n$, where the integral does not exist, is at our disposal. Likewise, in our case these moments are given by eq. (12) and do not behave uniformly for $|n| \rightarrow \infty$. Especially, they grow exponentially along \mathcal{C}_1 . Therefore, we will use the ‘textbook contour’ \mathcal{C}_0 in the following and, with $\phi = \pi/2$, eq. (18) simplifies to

$$F(x) = \frac{1}{\pi} \int_0^\infty dz \text{Re} \left[x^{-c-iz} F_{n=c+iz} \right] . \quad (19)$$

We have applications in mind where $F_n = f_{i/p,n} h_{an}$, see eq. (15), and the numerical evaluation of the moments h_{an} in eq. (12) is *very* time-consuming. Taking a different upper limit z_{max} of the numerical z -integration or number of points for the integral at each step in the integration process is practically unfeasible in such a case. Instead, we want to fix z_{max} at a value as small as possible in order to allow for an evaluation of eq. (19) with a rather small number of fixed moments.

In this context, it is useful to consider that part of the n -dependent inversion integrand, of which the analytical continuations are known together with the behaviour at large n , namely the parton densities and their evolution. Inspection of eq. (12) suggests that h_{an} does not rise strongly with z along \mathcal{C}_0 . Hence the large- n behaviour of the parton densities $f_{i/p,n}$ can be employed to estimate the convergence of the complete integral in eq. (19) with F_n given by eq. (15). A typical ansatz for the parton distribution functions of the proton at some reference scale μ_0^2 , denoted by $f_{i/p}(\xi)$, is given by [7, 9]

$$\xi f_{i/p}(\xi) = A \xi^\alpha (1 - \xi)^\beta (1 + \gamma \sqrt{\xi} + \dots) . \quad (20)$$

The coefficients β can be estimated roughly by their counting rule values, e.g. $\beta_{\text{val}} \approx 3$, $\beta_{\text{glue}} \approx 5$. The Mellin transform of eq. (20) reads simply

$$f_{i/p,n} = A [B(\alpha + n - 1, \beta + 1) + \gamma B(\alpha + n - 1/2, \beta + 1) + \dots] \quad (21)$$

with the Euler Beta-function B . If β is a positive integer, then this equation simplifies to

$$f_{i/p,n} = \frac{A \beta!}{(\alpha + n - 1)(\alpha + n) \dots (\alpha + n + \beta - 1)} + \dots = \mathcal{O}(1/n^{\beta+1}) \text{ for } n \rightarrow \infty . \quad (22)$$

The evolution of these input moments is known analytically for arbitrary complex n [10], and the kernel $K_{ij,n}(\mu^2, \mu_0^2)$ in

$$f_{i/p,n}(\mu^2) = K_{ij,n}(\mu^2, \mu_0^2) f_{j/p,n}(\mu_0^2) \quad (23)$$

generally leads to a slightly faster decrease of $f_{i/p,n}$ for large n at $\mu^2 > \mu_0^2$. Hence a fall-off like $1/n^4$ can be safely used to estimate the practically required upper limit in eq. (19).

For this purpose, we have numerically determined the upper limit z_{max} sufficient to reach a 1% accuracy of the Mellin inversion for the toy function $F(x) = x^{-1}(1-x)^3$. The results are displayed in table 1 for selected values of x . The rightmost pole is at $n_{max} = 1$, and we have chosen $c = 1.5$. The larger c is, the more $F_{n=c+iz}$ is flattened. Hence too large a value of c leads to an undesired rise of z_{max} at small x , where F_n is integrated after multiplication with a rapidly oscillating function in eq. (19). Practically, $c - n_{max} \simeq 0.5$ works well for all x -values of interest here, implying $c \simeq 1.8$ for realistic small- ξ parton densities [7, 9].

x	10^{-4}	10^{-3}	0.01	0.03	0.1	0.3	0.8
z_{max}	6.0	5.5	4.5	4.0	3.5	5.0	8.0

Table 1: *Upper limits z_{max} numerically sufficient for a 1% accuracy of the Mellin inversion from eq. (19) for the function $F(x) = x^{-1}(1-x)^3$ with $c = 1.5$.*

The integral eq. (19), truncated at z_{max} , can now be performed by using a sufficiently large number of fixed support points, e.g. by a sum of 8-point Gaussian quadratures, see [11] for the weights and support points. In this way, everything except for the input- B -functions varied in a fit of the parton distribution functions is fixed; especially the time-consuming part of the kernels in eq. (23) and the moments h_{an} of the partonic cross sections from eq. (12) can be determined once and then used unchanged in the calculation of physical observables for various parton densities.

4 Application to Jet Physics at HERA

To illustrate how the Mellin transform method can be used to fit the gluon density $f_{g/p}$, the gluon-induced (2+1)-jet cross sections were calculated in several bins for HERA energies of 820 GeV protons and 27.6 GeV electrons. Quark contributions were set to zero explicitly in the parton distribution function to reduce the number of moments needed for this case study.

The program PROJET [12] based on the NLO matrix elements from [13, 14] was used, this allows to calculate jet cross sections in LO and NLO in the modified JADE scheme defined in the following way [15]:

- Define a *precluster* of longitudinal momentum p_r given by the missing longitudinal momentum of the event.

- Apply the JADE cluster algorithm [16] to the set of momenta $\{p_1, \dots, p_n, p_r\}$, where p_1, \dots, p_n are the momenta of the hadrons visible in the detector. The resolution criterion is $s_{ij} = 2p_i p_j > y_{cut} M^2$. Here M^2 is a mass scale and y_{cut} is the resolution parameter.

In the case of a theoretical calculation, p_r is directly given by the momentum fraction of the proton not carried by the incident parton, and p_1, \dots, p_n are the momenta of the partons in the final state. In the following, we choose W^2 , the squared total hadronic energy, as the mass scale M^2 , since the proton remnant is included in the jet definition.

The integration routine used in PROJET is VEGAS [17, 18]. As is desirable for an experimental measurement, the phase space was binned in Q^2 and x_B according to eq. (8); the bins are given in tables 2 and 3. In addition, the following typical H1 detector cuts were applied, for which the motivation is explained in detail in [19]:

- The invariant mass squared of the hadronic system W^2 was required to be larger than 5000 GeV².
- The jet resolution cut y_{cut} was set to 0.02. Lowering this value significantly below 0.01 causes NLO corrections to dominate and leads to unphysical cross sections. It is important to note that $\xi \geq y_{cut}$ as a consequence of the applied modified JADE algorithm. The region $\xi > 0.01$ is however very interesting [20] for a precise determination of $f_{g/p}$, see also [21].
- The jets were required to lie in the polar angle range of $10^\circ \leq \theta_{jet} \leq 145^\circ$.
- For bins with $Q^2 \leq 100 \text{ GeV}^2$, the scattered electron had to have an energy of $E_{\nu'} \geq 14 \text{ GeV}$ and the polar angle had to lie within the range of $160^\circ \leq \theta_{\nu'} \leq 172.5^\circ$.
- In the bins with $Q^2 \geq 100 \text{ GeV}^2$, the scaled photon energy y in the proton rest system had to be $y \leq 0.7$ and the scattered electron was required to have $10^\circ \leq \theta_{\nu'} \leq 148^\circ$.

In this list, angles and energies are defined in the laboratory frame, and angles are given with respect to the direction of the incoming proton. For each bin, 32 complex Mellin moments were calculated according to the prescription described in Section 2, cf. eq. (12). In all calculations, α_s was computed to second order, and the NLO gluon distribution function of [7] was employed.

A good convergence of the numerical calculations was found for $c = 1.8$, $\phi = \pi/2$ and $z_{max} = 9$, with a higher density of support points at lower z , as the influence is greatest there. For comparison, the cross section was also calculated directly, see eqs. (6), (7), (8). After inverting the product of the hard subprocess and evolved gluon density moments at the average Q^2 , the results were found to coincide at the per cent level. The detailed results can be found in tables 2 and 3. In most bins, convergence was reached at $z_{max} = 3$ (corresponding to 16 moments), the additional moments were used for safety. The convergence of the LO cross section was much faster

Q^2 [GeV ²]	x_B									
	$10^{-4} \dots 1$		$10^{-3} \dots 1$		$10^{-2} \dots 1$		$10^{-1} \dots 1$			
10 ... 14	62.80	61.64	28.09	28.74	—	—	—	—	—	—
14 ... 18	70.64	69.72	50.95	49.97	—	—	—	—	—	—
18 ... 25	85.82	84.89	71.03	69.80	—	—	—	—	—	—
25 ... 40	109.9	108.8	101.9	101.1	—	—	—	—	—	—
40 ... 100	—	—	123.8	124.4	14.51	14.43	—	—	—	—
100 ... 300	—	—	31.96	32.18	14.69	14.76	—	—	—	—
300 ... 700	—	—	28.97	29.23	25.18	25.42	—	—	—	—
700 ... 4000	—	—	—	—	10.22	10.12	0.96	0.93	—	—

Table 2: Comparison of cross sections with LO matrix elements³ (in [pb]) obtained by integrating directly (left columns) or using the Mellin transform method (right columns).

Q^2 [GeV ²]	x_B									
	$10^{-4} \dots 1$		$10^{-3} \dots 1$		$10^{-2} \dots 1$		$10^{-1} \dots 1$			
10 ... 14	58.48	57.25	26.60	26.00	—	—	—	—	—	—
14 ... 18	66.57	65.90	47.22	46.69	—	—	—	—	—	—
18 ... 25	82.48	81.65	67.99	66.87	—	—	—	—	—	—
25 ... 40	108.1	107.4	100.4	99.71	—	—	—	—	—	—
40 ... 100	—	—	126.1	125.6	14.07	13.96	—	—	—	—
100 ... 300	—	—	34.86	34.52	15.51	15.31	—	—	—	—
300 ... 700	—	—	31.34	31.51	27.01	27.19	—	—	—	—
700 ... 4000	—	—	—	—	11.18	11.19	0.99	0.97	—	—

Table 3: Comparison of NLO cross sections (in [pb]) obtained by integrating directly (left columns) or using the Mellin transform method (right columns).

than in the NLO case, as for a given number of support points in VEGAS, the LO integration is more accurate due to the simpler integration kernel. The method works well for both LO and NLO.

The number of points in the Monte Carlo integration was chosen such that the error returned by VEGAS was less than 1%. This number is, however, only a rough estimate [17, 18], and the achieved accuracy was studied by repeating the calculation for different random number generator seeds. The direct integrations performed here had a statistical variation of 2–3%. The partonic cross section from the Mellin transform method is implicitly integrated repeatedly by the calculation of the moments, which smoothes out statistical variations. The results were found

³Here, ‘LO’ means that the matrix elements were calculated in LO, but α_s and the parton distribution functions in NLO to facilitate a comparison with the results of table 3. For a physically meaningful comparison of the LO with the NLO, α_s and the parton distribution functions should be calculated in LO, if they are used in conjunction with the LO matrix elements.

to be more stable than the direct integration, which varied around the result obtained by the moment inversion. Even drastic errors of single moments or setting single moments to zero could be tolerated and led to a reproducible result. We conclude that this method is numerically very stable and that the accuracy is of the order of 1%. Increasing the accuracy requires increasing the number of support points for the integration, which would result in a dramatic increase in CPU time⁴. One has to keep in mind that an additional error source arises from the Mellin transform method, as for each experimental bin in x one has to calculate the difference of the cross sections depending on the bin boundaries in eq. (9), leading to error propagation. A strategy for bin optimization is under study.

5 Summary

We have outlined a new method, based on the Mellin transform for the fast evaluation of the convolution of a parton-level cross section with a parton density, which works for cross sections not showing a simple factorization behaviour. The method can be the basis for a fit of the gluon density from experimental data for the (2+1)-jet cross section in deeply inelastic electron–proton scattering, but it is also suitable for more complicated observables. It has been explicitly shown by a numerical study using realistic experimental cuts, that the method works in practice with a sufficiently high accuracy.

Acknowledgements

It is a pleasure to thank G. Kramer for a critical reading of the manuscript and R. Nisius for many helpful discussions. This work was supported in part by the Bundesministerium für Bildung und Forschung. M.H. gratefully acknowledges support by the Studienstiftung des deutschen Volkes.

References

- [1] A. Mendez, Nucl. Phys. B145 (1978) 199.
- [2] H1 Collaboration, S. Aid et al., preprint DESY 95-086 (1995).
- [3] S. Catani, Y.L. Dokshitzer and B.R. Webber, Phys. Lett. B285 (1992) 291.
- [4] B.R. Webber, J. Phys. G19 (1993) 1567.

⁴The numerical calculation of one moment needed about 2 minutes of CPU time on an SGI Challenge processor in LO, and about 20 minutes in NLO.

- [5] R. Courant and D. Hilbert, *Methoden der Mathematischen Physik*, Springer Verlag, Berlin, 1924.
- [6] M. Glück, E. Reya and A. Vogt, Z. Phys. C53 (1992) 127.
- [7] M. Glück, E. Reya and A. Vogt, preprint DESY 94-206 (1994) and Univ. Dortmund preprint DO-TH 94/24, to appear in Z. Phys. C.
- [8] M. Glück, E. Reya and A. Vogt, Phys. Rev. D45 (1992) 3968, D46 (1993) 1973.
- [9] A.D. Martin, W.J. Stirling and R.G. Roberts, Phys. Rev. D50 (1994) 6734, Rutherford Appleton Laboratory preprint RAL-95-021 (1995).
- [10] M. Glück, E. Reya and A. Vogt, Z. Phys. C48 (1990) 471.
- [11] M. Abramowitz and I.A. Stegun (eds.), *Handbook of Mathematical Functions*, National Bureau of Standards, 1964.
- [12] D. Graudenz, PROJET 4.13 manual, preprint CERN-TH.7420/94 (November 1994).
- [13] D. Graudenz, Phys. Lett. B256 (1991) 518.
- [14] D. Graudenz, Phys. Rev. D49 (1994) 3291.
- [15] D. Graudenz and N. Magnussen, in: Proceedings of the HERA Workshop 1991, DESY (eds. W. Buchmüller, G. Ingelman).
- [16] JADE Collaboration, W. Bartel et al., Z. Phys. C33 (1986) 23.
- [17] G. Lepage, J. Comput. Phys. 27 (1978) 1992.
- [18] G. Lepage, Cornell preprint CLNS-80/447 (1980).
- [19] H1 Collaboration, T. Ahmed et al., Phys. Lett. B346 (1995) 415.
- [20] W.J. Stirling, talk presented on the Workshop on Deep Inelastic Scattering and QCD, Paris, April 1995.
- [21] W. Vogelsang and A. Vogt, Rutherford Appleton Laboratory preprint CCL-TR-95-004 and preprint DESY 95-096 (1995).

The Mellin Transform Technique for the Extraction of the Gluon Density

D. Graudenz¹, M. Hampel², A. Vogt^{3*}, Ch. Berger²

¹Theoretical Physics Division, CERN
CH-1211 Geneva 23, Switzerland

²I. Physikalisches Institut, RWTH Aachen
D-52056 Aachen, Germany

³Deutsches Elektronen-Synchrotron DESY
D-22603 Hamburg, Germany

Abstract

A new method is presented to determine the gluon density in the proton from jet production in deeply inelastic scattering. By using the technique of Mellin transforms not only for the solution of the scale evolution equation of the parton densities but also for the evaluation of scattering cross sections, the gluon density can be extracted in next-to-leading order QCD. The method described in this paper is, however, more general, and can be used in situations where a repeated fast numerical evaluation of scattering cross sections for varying parton distribution functions is required.

CERN-TH/95-149

June 1995

*On leave of absence from Sektion Physik, Universität München, D-80333 Munich, Germany.

Electronic mail addresses: Dirk.Graudenz@cern.ch, Hampel@desy.de, avogt@x4u2.desy.de, Berger@rwth-aachen.de.

1 Introduction

One of the main goals of experiments at the electron–proton collider HERA is the precise determination of the gluon density $f_{g/p}(\xi, \mu^2)$ in the proton for various gluon momentum fractions ξ and factorization scales μ . In addition to the indirect method of extracting $f_{g/p}$ from the scaling violation of the structure function F_2 , direct methods such as heavy quark and jet production have been studied.

In the QCD–improved parton model, the electron–proton scattering cross section σ is generically given by a convolution of process-independent parton densities $f_{q/p}$ for (anti-)quarks and $f_{g/p}$ for gluons with corresponding mass-factorized parton-level cross sections σ_q and σ_g :

$$\sigma = \int d\xi \left[f_{q/p}(\xi, \mu^2) \sigma_q(\xi, \mu^2) + f_{g/p}(\xi, \mu^2) \sigma_g(\xi, \mu^2) \right]. \quad (1)$$

Besides the indicated dependence on ξ and μ , σ_q and σ_g also depend on other variables such as the absolute electron four-momentum transfer squared Q^2 and the momenta of the outgoing partons¹.

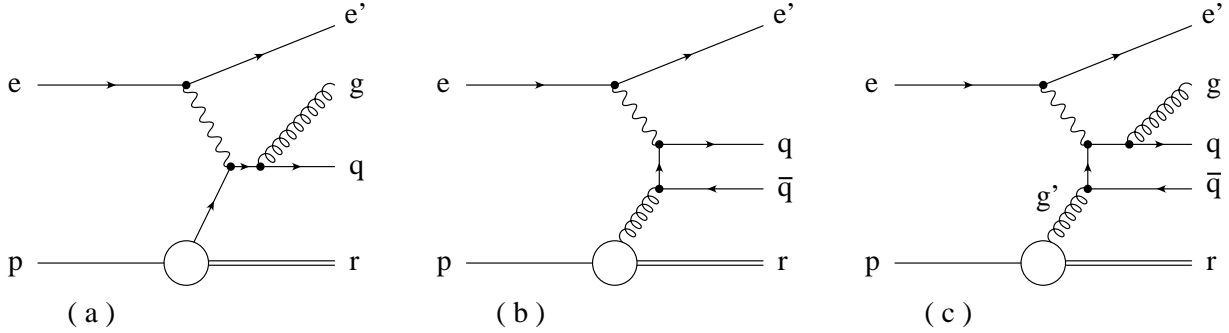


Figure 1: *Generic Feynman diagrams for the leading-order processes of QCD Compton scattering (a) and photon-gluon fusion (b), and an example for a diagram corresponding to a next-to-leading order real correction (c).*

In leading order (LO), the prescription for the extraction of $f_{g/p}$ from jet cross sections in deeply inelastic scattering reactions is very intuitive, because σ_q can be identified with the parton-model cross section σ_C for the so-called *QCD Compton scattering* process (fig. 1a), and σ_g with the parton-model cross section σ_F for the *photon-gluon fusion* reaction (fig. 1b). Explicit expressions can be found in [1]. Experimentally the outgoing partons from the hard scattering reactions are identified with jets. The QCD Compton scattering and photon-gluon fusion reactions lead to (2+1)-jet final states, where the notation accounts for the two outgoing jets from the hard scattering process and the jet in the proton fragmentation region. The calculated contribution

¹Here and in the following we do not explicitly display the dependence on the renormalization scale.

$\sigma_{C,2+1}^{\text{LO}} = \int d\xi f_{q/p}(\xi, \mu^2) \sigma_C(\xi)$ from Compton scattering can be subtracted from the measured cross section

$$\sigma_{2+1}^{\text{LO}} = \int d\xi \left[f_{q/p}(\xi, \mu^2) \sigma_C(\xi) + f_{g/p}(\xi, \mu) \sigma_F(\xi) \right], \quad (2)$$

and thus $f_{g/p}(\xi, \mu^2)$ can be determined in LO by a direct unfolding, since in this case ξ can be expressed in terms of measurable quantities as $\xi = x_B (1 + \hat{s}/Q^2)$, where x_B is the Bjorken scaling variable and \hat{s} is the invariant mass squared of the system of the two current jets. An analysis based on this principle has recently been presented by the H1 Collaboration [2].

In next-to-leading order (NLO) this simple picture is destroyed. Aside from the virtual corrections to the Born processes in figs. 1a and b, real corrections have to be added; diagrams of the type shown in fig. 1c can also lead to (2+1)-jet configurations: if the gluon g attached to the outgoing quark is soft or collinear to the quark, the diagram constitutes a correction to the photon–gluon fusion process. If, on the other hand, this gluon is hard and the outgoing antiquark \bar{q} is soft or collinear to the incoming gluon g' , then this configuration can be said to be a correction to the QCD Compton scattering reaction. In the latter case, the collinear or soft antiquark forms a jet with the proton remnant r , and the cross section has to be integrated over all momenta of the antiquark according to a specific jet definition scheme. Collinear singularities that do not cancel against corresponding singularities from the virtual corrections have to be absorbed into renormalized parton densities. Depending on the factorization scheme chosen, finite subtracted pieces remain. The factorization theorems of perturbative QCD guarantee that the cross section can be written in the form of eq. (1). However, beyond the leading order, the arbitrary momentum of collinear partons renders the variable ξ unobservable, because the mass-factorized parton-level cross sections are in general distributions, not regular functions, and the simple and straightforward method described above can therefore not be applied. A physical consequence is that the distinction between the QCD Compton and photon–gluon fusion processes becomes meaningless. Related to this is the fact that quark and gluon densities mix in the Altarelli–Parisi scale evolution.

A determination of the gluon density in NLO is very desirable. In LO the partonic cross sections σ_q and σ_g (in short denoted by σ_i) do not depend on μ , as already indicated in eq. (2), and the $f_{i/p}$ (as short-hand for $f_{q/p}$ and $f_{g/p}$) are the solutions of the LO Altarelli–Parisi evolution equation, where the leading logarithmic terms in the scale μ are summed up. In any finite order of perturbation theory, the scattering cross section σ depends explicitly on the factorization scale μ , this scale dependence being due to uncalculated higher-order terms. The scale dependence is particularly strong in the LO case, because there no compensation can take place between $f_{i/p}$ and σ_i . To a great extent this problem is, for many processes, reduced in NLO, where explicit terms $\sim \ln \mu^2$ in σ_i compensate the μ -dependence of $f_{i/p}$ such that the variation is of higher order in the strong coupling constant α_s . For reliable theoretical predictions, a NLO analysis of scale-dependent quantities is therefore mandatory.

The only way to achieve a direct NLO determination of $f_{g/p}$ is to parametrize the function

$f_{g/p}$ at a given scale μ_0 , to evolve it then to a value of μ where the cross section is measured, say $\mu = Q$, and to fit the parameters of $f_{g/p}$ with respect to suitable infrared safe observables, e.g. the (2+1)-jet cross section in various bins of x_B . A severe practical problem is that the cross section σ has to be evaluated repeatedly for every choice of parameters for $f_{g/p}$. Monte Carlo methods allow the application of arbitrary cuts on final-state particle momenta, as is necessary in order to take detector acceptance cuts properly into account, but these methods are prohibitively slow. A fast numerical method for the repeated application of this procedure is indispensable, and will be developed in this paper.

The paper is organized as follows. The new method is formally derived in Section 2. Details of the Mellin transform relevant to the application of the method are discussed in Section 3. Finally, an explicit numerical example is given in Section 4 for the case of jet cross sections in deeply inelastic electron–proton scattering, where it is shown that the method is operational in practice when realistic acceptance cuts are taken into account. The paper closes with a short summary.

2 The Mellin Transform Technique for Non-Factorizing Cross Sections

The Mellin transform technique allows for a quick numerical evaluation of integrals of the form

$$\Sigma(x_B) = \int_{x_B}^1 \frac{d\xi}{\xi} f_{i/p}(\xi) \sigma_i\left(\frac{x_B}{\xi}, x_B\right) \quad (3)$$

in the case where σ_i is independent of its second argument x_B , on the basis of the moments defined by

$$F_n \equiv \int_0^1 \frac{dx}{x} x^n F(x) \quad (4)$$

for an arbitrary function F and (complex) n . The moments of the function Σ are then given by

$$\Sigma_n = f_{i/p,n} \sigma_{i,n}. \quad (5)$$

The functional dependence of Σ can be recovered from the moments Σ_n by an inverse Mellin transform. An expression of the form of eq. (3) will be called to be of the *factorizable type* if the only dependence on x_B in the arguments of σ_i is via x_B/ξ . In the application which we have in mind, $f_{i/p}$ is a parton density, whereas σ_i is an expression for a mass-factorized parton-level scattering cross section. In general, acceptance cuts and non-factorizable jet algorithms (cf. the discussion in [3, 4]) introduce an explicit dependence of σ_i on x_B . Moreover, the expression for $\Sigma(x_B)$ is integrated over a certain range of x_B . This might suggest that the Mellin transform technique cannot be applied. However, this is not the case. In the following we outline a method that allows the use of this technique.

The cross section differential in x_B can be written in the form

$$\Sigma(x_B) = \int_{x_B}^1 \frac{d\xi}{\xi} f_{i/p}(\xi, \mu^2) \sigma_i\left(\frac{x_B}{\xi}, x_B, \mu^2\right), \quad (6)$$

where

$$\sigma_i\left(\frac{x_B}{\xi}, x_B, \mu^2\right) = \int_{V_{x_B}} dT \hat{\sigma}_i\left(\frac{x_B}{\xi}, x_B, T, \mu^2\right). \quad (7)$$

Here we have made the dependence on the factorization scale μ explicit. The set T of variables contains all other integration variables besides x_B , i.e. the other electron variables including Q^2 and the momenta of the outgoing partons (or jets); and V_{x_B} is the phase space region over which these variables are integrated. Thus, V_{x_B} includes all acceptance and jet cuts, as well as the range in Q^2 for the specified x_B . $\hat{\sigma}_i$ is the cross section differential in all variables including T , whereas σ_i is the integration kernel to be convoluted with $f_{i/p}$ to yield Σ . The explicit dependence on x_B of $\hat{\sigma}_i(x_B/\xi, x_B, T, \mu^2)$ and $\sigma_i(x_B/\xi, x_B, \mu^2)$ (not just via the ratio x_B/ξ) is a consequence of the (finite) factorization breaking terms².

It is assumed that the factorization scale μ is chosen independently from the variables T ; in particular, μ should not depend on the integration variable Q^2 , which is integrated over a certain range $[Q_0^2, Q_1^2]$. μ it may be set to some intermediate value. In any case, this is not a strong restriction, because the parton densities depend only logarithmically on the factorization scale, and moreover the scale dependence is compensated by a corresponding term in the mass-factorized parton-level scattering cross section, so that the change is of higher order in α_s . For simplicity of notation, we drop the argument μ^2 in the following.

Now let (for a fixed Q^2 -bin) a_1, \dots, a_k be the experimental boundaries of the intervals in the variable x_B for which the cross sections are measured. To proceed, we define

$$\Sigma_a \equiv \int_a^1 dx_B \Sigma(x_B). \quad (8)$$

The integral over a specified interval $[a_i, a_{i+1}]$ in x_B is then simply given by

$$\int_{a_i}^{a_{i+1}} dx_B \Sigma(x_B) = \Sigma_{a_i} - \Sigma_{a_{i+1}}. \quad (9)$$

In a fit of the function $f_{i/p}$, the integrals in eqs. (6), (7), (8) have to be evaluated repeatedly. In general, the x_B , ξ and T -integrations are performed by a time-consuming Monte Carlo integration in order to implement all cuts. In particular, the (x_B, Q^2) -plane is divided into several bins which do not change during the fitting procedure. The method requires that a certain set of moments is calculated for every bin in the (x_B, Q^2) -plane. The steps to be followed to determine the Σ_a are:

²It should be kept in mind that the infinite terms related to infrared and collinear singularities still factorize in the standard form so that universal parton densities can be defined. This property is not spoiled by acceptance cuts and non-factorizing jet definition schemes.

- Define a function

$$h_a(u) \equiv \begin{cases} \int_a^{a/u} dx_B \sigma_i \left(\frac{x_B}{a/u}, x_B \right), & \text{if } u \geq a \\ 0, & \text{if } u < a \end{cases} \quad (10)$$

and its moments in the variable u

$$h_{an} \equiv \int_0^1 \frac{du}{u} u^n h_a(u). \quad (11)$$

It is easy to prove that an explicit expression for h_{an} is

$$h_{an} = \int_a^1 dx_B \int_{x_B}^1 \frac{d\xi}{\xi} \left(\frac{a}{\xi} \right)^n \sigma_i \left(\frac{x_B}{\xi}, x_B \right). \quad (12)$$

The h_{an} are thus the Σ_a with the parton density $f_{i/p}(\xi)$ replaced by $(a/\xi)^n$. They can be determined numerically by means of a Monte Carlo integration. In general, for complex n , the quantity $(a/\xi)^n$ has to be split into its real and imaginary part.

- Define

$$\Sigma_{ab} \equiv \int_a^1 \frac{d\xi}{\xi} f_{i/p}(\xi) h_b \left(\frac{a}{\xi} \right) \quad (13)$$

and determine the moments of Σ_{ab} with respect to the variable a :

$$\tilde{\Sigma}_{nb} \equiv \int_0^1 \frac{da}{a} a^n \Sigma_{ab}. \quad (14)$$

Obviously, $\Sigma_a = \Sigma_{aa}$. The key relation of our method is

$$\tilde{\Sigma}_{nb} = f_{i/p,n} h_{bn}, \quad (15)$$

and can be proved in the following way:

$$\begin{aligned} \tilde{\Sigma}_{nb} &= \int_0^1 \frac{da}{a} a^n \int_a^1 \frac{d\xi}{\xi} f_{i/p}(\xi) h_b \left(\frac{a}{\xi} \right) \\ &= \int_0^1 \frac{d\xi}{\xi} f_{i/p}(\xi) \int_0^\xi \frac{da}{a} a^n h_b \left(\frac{a}{\xi} \right) \\ &= \int_0^1 \frac{d\xi}{\xi} \xi^n f_{i/p}(\xi) \int_0^1 \frac{du}{u} u^n h_b(u) \\ &= f_{i/p,n} h_{bn}. \end{aligned} \quad (16)$$

- For a given parametrization of $f_{i/p}$ in terms of its moments $f_{i/p,n}$ the cross section Σ_a can be determined by forming the moments $\tilde{\Sigma}_{na} = f_{i/p,n} h_{an}$ and a subsequent inverse Mellin transform in the variable n , evaluated at a .

The Mellin transform method in the case of non-factorizing cross sections introduces the inconvenience that the moments h_{an} have to be determined for every interval boundary a separately. Due to the large number of repeated cross section evaluations in the fitting procedure, however, this method is far more efficient than a direct integration of the integrals in eqs. (6), (7), (8) for every parametrized parton density.

3 From Parton Moments to Observables

Let us now consider the inverse transformation of the moments given by eq. (4), which is a special case of the general Mellin transformation for functions $F(x)$ vanishing identically at $x > 1$. If $F(x)$ is piecewise smooth for $x > 0$, the corresponding Mellin inversion reads

$$F(x) = \frac{1}{2\pi i} \int_{c-i\infty}^{c+i\infty} dn x^{-n} F_n, \quad (17)$$

where the real number c has to be chosen such that $\int_0^1 dx x^{c-1} F(x)$ is absolutely convergent [5]. Hence c has to lie to the right of the rightmost singularity n_{max} of F_n . The contour of the integration in eq. (17) is displayed in fig. 2 and denoted by C_0 . Also shown is a deformed route C_1 , yielding the same result as long as no singularities n_i of F_n are enclosed by $C_0 - C_1$. For example, for the LO and NLO evolution of structure functions, the n_i are real with $n_i < n_{max} < c$, and this requirement is fulfilled automatically.

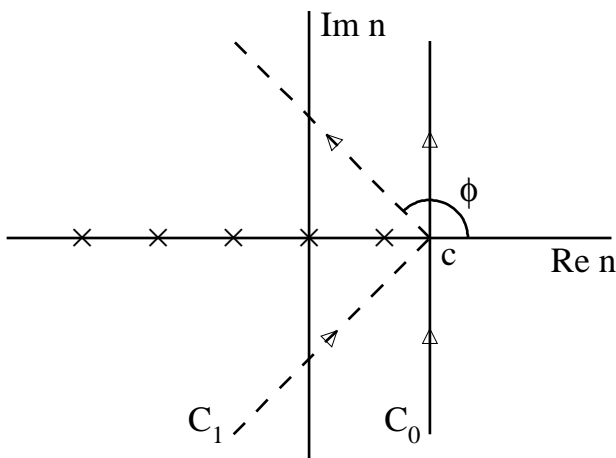


Figure 2: Integration contours of the Mellin inversion in eq. (17), leading to the inversion formulae of eqs. (18) and (19) for the routes C_0 and C_1 , respectively. The crosses schematically denote the singularities of F_n .

It is useful to rewrite eq. (17) as an integration over a real variable. We are concerned with functions obeying $F_n^* = F_{n^*}$, where ‘ $*$ ’ denotes the complex conjugation. Then it is easy to show that eq. (17) yields, for the contour characterized by the abscissa c and the angle ϕ in fig. 2:

$$F(x) = \frac{1}{\pi} \int_0^\infty dz \operatorname{Im} \left[\exp(i\phi) x^{-c-z \exp(i\phi)} F_{n=c+z \exp(i\phi)} \right]. \quad (18)$$

It is obvious from the discussion given above that the integral does not depend on c and ϕ . However, for an efficient numerical evaluation a suitable choice of these parameters is very useful. For example, it is advantageous to choose $\phi > \pi/2$ in case F_n is a known analytical function,

especially if this function does not fall off very rapidly for $|n| \rightarrow \infty$. The factor $\exp\left(z \log \frac{1}{x} \cos \phi\right)$ then introduces an exponential dampening of the integrand (which rapidly oscillates at small x) with increasing z , thereby allowing for a smaller upper limit z_{max} in the numerical implementation of eq. (18). This procedure has been employed for the inversion of moments of parton densities and structure functions for the proton and the photon, e.g. in [6, 7] and [8], respectively.

In general, however, the moments of the partonic cross section can only be calculated numerically using eq. (4), because no analytic continuation to small $\text{Re } n$, where the integral does not exist, is at our disposal. Likewise, in our case these moments are given by eq. (12) and do not behave uniformly for $|n| \rightarrow \infty$. Especially, they grow exponentially along C_1 . Therefore, we will use the ‘textbook contour’ C_0 in the following and, with $\phi = \pi/2$, eq. (18) simplifies to

$$F(x) = \frac{1}{\pi} \int_0^\infty dz \text{Re} \left[x^{-c-iz} F_{n=c+iz} \right] . \quad (19)$$

We have applications in mind where $F_n = f_{i/p,n} h_{an}$, see eq. (15), and the numerical evaluation of the moments h_{an} in eq. (12) is *very* time-consuming. Taking a different upper limit z_{max} of the numerical z -integration or number of points for the integral at each step in the integration process is practically unfeasible in such a case. Instead, we want to fix z_{max} at a value as small as possible in order to allow for an evaluation of eq. (19) with a rather small number of fixed moments.

In this context, it is useful to consider that part of the n -dependent inversion integrand, of which the analytical continuations are known together with the behaviour at large n , namely the parton densities and their evolution. Inspection of eq. (12) suggests that h_{an} does not rise strongly with z along C_0 . Hence the large- n behaviour of the parton densities $f_{i/p,n}$ can be employed to estimate the convergence of the complete integral in eq. (19) with F_n given by eq. (15). A typical ansatz for the parton distribution functions of the proton at some reference scale μ_0^2 , denoted by $f_{i/p}(\xi)$, is given by [7, 9]

$$\xi f_{i/p}(\xi) = A \xi^\alpha (1 - \xi)^\beta (1 + \gamma \sqrt{\xi} + \dots) . \quad (20)$$

The coefficients β can be estimated roughly by their counting rule values, e.g. $\beta_{\text{val}} \approx 3$, $\beta_{\text{glue}} \approx 5$. The Mellin transform of eq. (20) reads simply

$$f_{i/p,n} = A [B(\alpha + n - 1, \beta + 1) + \gamma B(\alpha + n - 1/2, \beta + 1) + \dots] \quad (21)$$

with the Euler Beta-function B . If β is a positive integer, then this equation simplifies to

$$f_{i/p,n} = \frac{A \beta!}{(\alpha + n - 1)(\alpha + n) \dots (\alpha + n + \beta - 1)} + \dots = \mathcal{O}(1/n^{\beta+1}) \text{ for } n \rightarrow \infty . \quad (22)$$

The evolution of these input moments is known analytically for arbitrary complex n [10], and the kernel $K_{ij,n}(\mu^2, \mu_0^2)$ in

$$f_{i/p,n}(\mu^2) = K_{ij,n}(\mu^2, \mu_0^2) f_{j/p,n}(\mu_0^2) \quad (23)$$

generally leads to a slightly faster decrease of $f_{i/p,n}$ for large n at $\mu^2 > \mu_0^2$. Hence a fall-off like $1/n^4$ can be safely used to estimate the practically required upper limit in eq. (19).

For this purpose, we have numerically determined the upper limit z_{max} sufficient to reach a 1% accuracy of the Mellin inversion for the toy function $F(x) = x^{-1}(1-x)^3$. The results are displayed in table 1 for selected values of x . The rightmost pole is at $n_{max} = 1$, and we have chosen $c = 1.5$. The larger c is, the more $F_{n=c+iz}$ is flattened. Hence too large a value of c leads to an undesired rise of z_{max} at small x , where F_n is integrated after multiplication with a rapidly oscillating function in eq. (19). Practically, $c - n_{max} \simeq 0.5$ works well for all x -values of interest here, implying $c \simeq 1.8$ for realistic small- ξ parton densities [7, 9].

x	10^{-4}	10^{-3}	0.01	0.03	0.1	0.3	0.8
z_{max}	6.0	5.5	4.5	4.0	3.5	5.0	8.0

Table 1: *Upper limits z_{max} numerically sufficient for a 1% accuracy of the Mellin inversion from eq. (19) for the function $F(x) = x^{-1}(1-x)^3$ with $c = 1.5$.*

The integral eq. (19), truncated at z_{max} , can now be performed by using a sufficiently large number of fixed support points, e.g. by a sum of 8-point Gaussian quadratures, see [11] for the weights and support points. In this way, everything except for the input- B -functions varied in a fit of the parton distribution functions is fixed; especially the time-consuming part of the kernels in eq. (23) and the moments h_{an} of the partonic cross sections from eq. (12) can be determined once and then used unchanged in the calculation of physical observables for various parton densities.

4 Application to Jet Physics at HERA

To illustrate how the Mellin transform method can be used to fit the gluon density $f_{g/p}$, the gluon-induced (2+1)-jet cross sections were calculated in several bins for HERA energies of 820 GeV protons and 27.6 GeV electrons. Quark contributions were set to zero explicitly in the parton distribution function to reduce the number of moments needed for this case study.

The program PROJET [12] based on the NLO matrix elements from [13, 14] was used, this allows to calculate jet cross sections in LO and NLO in the modified JADE scheme defined in the following way [15]:

- Define a *precluster* of longitudinal momentum p_r given by the missing longitudinal momentum of the event.

- Apply the JADE cluster algorithm [16] to the set of momenta $\{p_1, \dots, p_n, p_r\}$, where p_1, \dots, p_n are the momenta of the hadrons visible in the detector. The resolution criterion is $s_{ij} = 2p_i p_j > y_{cut} M^2$. Here M^2 is a mass scale and y_{cut} is the resolution parameter.

In the case of a theoretical calculation, p_r is directly given by the momentum fraction of the proton not carried by the incident parton, and p_1, \dots, p_n are the momenta of the partons in the final state. In the following, we choose W^2 , the squared total hadronic energy, as the mass scale M^2 , since the proton remnant is included in the jet definition.

The integration routine used in PROJET is VEGAS [17, 18]. As is desirable for an experimental measurement, the phase space was binned in Q^2 and x_B according to eq. (8); the bins are given in tables 2 and 3. In addition, the following typical H1 detector cuts were applied, for which the motivation is explained in detail in [19]:

- The invariant mass squared of the hadronic system W^2 was required to be larger than 5000 GeV².
- The jet resolution cut y_{cut} was set to 0.02. Lowering this value significantly below 0.01 causes NLO corrections to dominate and leads to unphysical cross sections. It is important to note that $\xi \geq y_{cut}$ as a consequence of the applied modified JADE algorithm. The region $\xi > 0.01$ is however very interesting [20] for a precise determination of $f_{g/p}$, see also [21].
- The jets were required to lie in the polar angle range of $10^\circ \leq \theta_{jet} \leq 145^\circ$.
- For bins with $Q^2 \leq 100 \text{ GeV}^2$, the scattered electron had to have an energy of $E_{\nu} \geq 14 \text{ GeV}$ and the polar angle had to lie within the range of $160^\circ \leq \theta_{\nu} \leq 172.5^\circ$.
- In the bins with $Q^2 \geq 100 \text{ GeV}^2$, the scaled photon energy y in the proton rest system had to be $y \leq 0.7$ and the scattered electron was required to have $10^\circ \leq \theta_{\nu} \leq 148^\circ$.

In this list, angles and energies are defined in the laboratory frame, and angles are given with respect to the direction of the incoming proton. For each bin, 32 complex Mellin moments were calculated according to the prescription described in Section 2, cf. eq. (12). In all calculations, α_s was computed to second order, and the NLO gluon distribution function of [7] was employed.

A good convergence of the numerical calculations was found for $c = 1.8$, $\phi = \pi/2$ and $z_{max} = 9$, with a higher density of support points at lower z , as the influence is greatest there. For comparison, the cross section was also calculated directly, see eqs. (6), (7), (8). After inverting the product of the hard subprocess and evolved gluon density moments at the average Q^2 , the results were found to coincide at the per cent level. The detailed results can be found in tables 2 and 3. In most bins, convergence was reached at $z_{max} = 3$ (corresponding to 16 moments), the additional moments were used for safety. The convergence of the LO cross section was much faster

Q^2 [GeV ²]	x_B							
	$10^{-4} \dots 1$		$10^{-3} \dots 1$		$10^{-2} \dots 1$		$10^{-1} \dots 1$	
10 ... 14	62.80	61.64	28.09	28.74	—	—	—	—
14 ... 18	70.64	69.72	50.95	49.97	—	—	—	—
18 ... 25	85.82	84.89	71.03	69.80	—	—	—	—
25 ... 40	109.9	108.8	101.9	101.1	—	—	—	—
40 ... 100	—	—	123.8	124.4	14.51	14.43	—	—
100 ... 300	—	—	31.96	32.18	14.69	14.76	—	—
300 ... 700	—	—	28.97	29.23	25.18	25.42	—	—
700 ... 4000	—	—	—	—	10.22	10.12	0.96	0.93

Table 2: Comparison of cross sections with LO matrix elements³ (in [pb]) obtained by integrating directly (left columns) or using the Mellin transform method (right columns).

Q^2 [GeV ²]	x_B							
	$10^{-4} \dots 1$		$10^{-3} \dots 1$		$10^{-2} \dots 1$		$10^{-1} \dots 1$	
10 ... 14	58.48	57.25	26.60	26.00	—	—	—	—
14 ... 18	66.57	65.90	47.22	46.69	—	—	—	—
18 ... 25	82.48	81.65	67.99	66.87	—	—	—	—
25 ... 40	108.1	107.4	100.4	99.71	—	—	—	—
40 ... 100	—	—	126.1	125.6	14.07	13.96	—	—
100 ... 300	—	—	34.86	34.52	15.51	15.31	—	—
300 ... 700	—	—	31.34	31.51	27.01	27.19	—	—
700 ... 4000	—	—	—	—	11.18	11.19	0.99	0.97

Table 3: Comparison of NLO cross sections (in [pb]) obtained by integrating directly (left columns) or using the Mellin transform method (right columns).

than in the NLO case, as for a given number of support points in VEGAS, the LO integration is more accurate due to the simpler integration kernel. The method works well for both LO and NLO.

The number of points in the Monte Carlo integration was chosen such that the error returned by VEGAS was less than 1%. This number is, however, only a rough estimate [17, 18], and the achieved accuracy was studied by repeating the calculation for different random number generator seeds. The direct integrations performed here had a statistical variation of 2–3%. The partonic cross section from the Mellin transform method is implicitly integrated repeatedly by the calculation of the moments, which smoothes out statistical variations. The results were found

³Here, ‘LO’ means that the matrix elements were calculated in LO, but α_s and the parton distribution functions in NLO to facilitate a comparison with the results of table 3. For a physically meaningful comparison of the LO with the NLO, α_s and the parton distribution functions should be calculated in LO, if they are used in conjunction with the LO matrix elements.

to be more stable than the direct integration, which varied around the result obtained by the moment inversion. Even drastic errors of single moments or setting single moments to zero could be tolerated and led to a reproducible result. We conclude that this method is numerically very stable and that the accuracy is of the order of 1%. Increasing the accuracy requires increasing the number of support points for the integration, which would result in a dramatic increase in CPU time⁴. One has to keep in mind that an additional error source arises from the Mellin transform method, as for each experimental bin in x one has to calculate the difference of the cross sections depending on the bin boundaries in eq. (9), leading to error propagation. A strategy for bin optimization is under study.

5 Summary

We have outlined a new method, based on the Mellin transform for the fast evaluation of the convolution of a parton-level cross section with a parton density, which works for cross sections not showing a simple factorization behaviour. The method can be the basis for a fit of the gluon density from experimental data for the (2+1)-jet cross section in deeply inelastic electron–proton scattering, but it is also suitable for more complicated observables. It has been explicitly shown by a numerical study using realistic experimental cuts, that the method works in practice with a sufficiently high accuracy.

Acknowledgements

It is a pleasure to thank G. Kramer for a critical reading of the manuscript and R. Nisius for many helpful discussions. This work was supported in part by the Bundesministerium für Bildung und Forschung. M.H. gratefully acknowledges support by the Studienstiftung des deutschen Volkes.

References

- [1] A. Mendez, Nucl. Phys. B145 (1978) 199.
- [2] H1 Collaboration, S. Aid et al., preprint DESY 95-086 (1995).
- [3] S. Catani, Y.L. Dokshitzer and B.R. Webber, Phys. Lett. B285 (1992) 291.
- [4] B.R. Webber, J. Phys. G19 (1993) 1567.

⁴The numerical calculation of one moment needed about 2 minutes of CPU time on an SGI Challenge processor in LO, and about 20 minutes in NLO.

- [5] R. Courant and D. Hilbert, *Methoden der Mathematischen Physik*, Springer Verlag, Berlin, 1924.
- [6] M. Glück, E. Reya and A. Vogt, Z. Phys. C53 (1992) 127.
- [7] M. Glück, E. Reya and A. Vogt, preprint DESY 94-206 (1994) and Univ. Dortmund preprint DO-TH 94/24, to appear in Z. Phys. C.
- [8] M. Glück, E. Reya and A. Vogt, Phys. Rev. D45 (1992) 3968, D46 (1993) 1973.
- [9] A.D. Martin, W.J. Stirling and R.G. Roberts, Phys. Rev. D50 (1994) 6734, Rutherford Appleton Laboratory preprint RAL-95-021 (1995).
- [10] M. Glück, E. Reya and A. Vogt, Z. Phys. C48 (1990) 471.
- [11] M. Abramowitz and I.A. Stegun (eds.), *Handbook of Mathematical Functions*, National Bureau of Standards, 1964.
- [12] D. Graudenz, PROJET 4.13 manual, preprint CERN-TH.7420/94 (November 1994).
- [13] D. Graudenz, Phys. Lett. B256 (1991) 518.
- [14] D. Graudenz, Phys. Rev. D49 (1994) 3291.
- [15] D. Graudenz and N. Magnussen, in: Proceedings of the HERA Workshop 1991, DESY (eds. W. Buchmüller, G. Ingelman).
- [16] JADE Collaboration, W. Bartel et al., Z. Phys. C33 (1986) 23.
- [17] G. Lepage, J. Comput. Phys. 27 (1978) 1992.
- [18] G. Lepage, Cornell preprint CLNS-80/447 (1980).
- [19] H1 Collaboration, T. Ahmed et al., Phys. Lett. B346 (1995) 415.
- [20] W.J. Stirling, talk presented on the Workshop on Deep Inelastic Scattering and QCD, Paris, April 1995.
- [21] W. Vogelsang and A. Vogt, Rutherford Appleton Laboratory preprint CCL-TR-95-004 and preprint DESY 95-096 (1995).